Area and edge effects in radiometric forces

N. Selden, C. Ngalande, S. Gimelshein, and E. P. Muntz
University of Southern California, Los Angeles, California 90089, USA

A. Alexeenko
Purdue University, West Lafayette, Indiana 47907, USA

A. Ketsdever
Edwards AFB, California 93524, USA

(Received 5 January 2009; published 6 April 2009)

The radiometric force on several configurations of heated plates placed in a stagnant gas is examined experimentally, with a high-resolution thrust stand, and numerically using the direct simulation Monte Carlo method and a discrete ordinate solution of a model kinetic equation. A wide range of pressures from 0.006 to 6 Pa was examined, corresponding to Knudsen numbers from 20 to 0.02, in argon and helium test gases. The radiometric force, important in a number of emerging micro- and nanoscale applications, is shown to be mostly area dependent in the transitional regime where it reaches its maximum at $\mathrm{Kn} \sim 0.1$.

DOI: 10.1103/PhysRevE.79.041201 PACS number(s): 51.10.+y, 47.45.Dt, 47.45.Gx

The kinetic theory of gases predicts the existence of a force resulting from nonequilibrium temperature gradients in a fluid. This force on a surface, usually called radiometric, is induced by thermally driven gas flow where the local mean-free path is comparable to the flow gradient length scale. This makes radiometric forces important in various low-density environments as well as micro- and nanoscale systems. The radiometric forces may generally be created by various sources such as radiation or resistive heating. The repulsion and attraction of bodies induced by radiation received a great deal of attention from a number of prominent scientists in the 19th and 20th centuries [1]. The first published experiment was conducted by Bennet [2] who reported in 1792 the negative result of light directed to a paper vane suspended by a fiber thread in vacuum. At that time, he was unable to see any motion distinguishable from the effect of heat. The first successful experiment was conducted by Fresnel [3] who observed in 1825 a repulsion between two suspended foil vanes when sunlight was focused on them in a low-pressure container.

In the 1870s, Crookes [4,5] proposed different types of apparatus to investigate the radiometer effect; one of them became known as the Crookes radiometer. It consists of an airtight glass bulb containing a partial vacuum with a set of vanes mounted inside the bulb on a spindle; the vanes rotate when exposed to light or another heat source. Crookes incorrectly suggested that the force causing the vanes to move was due to photon pressure. This theory was originally supported by Maxwell who had predicted this force. Reynolds had initially proposed a reasoning based on surface outgassing, and then presented a more rigorous explanation based on kinetic theory [6]. According to the latter theory, the gas in the partially evacuated bulb is the main driving force responsible for the rotation of the vanes.

Reynolds also took part in the experiments conducted by Schuster [7] that turned up the first experimental evidence of gas forces being the dominant cause of the radiometric effect. In this experiment, the radiometer case was suspended by parallel fibers and light was directed onto the vanes. The radiometer case was pushed in the direction opposite the vanes, proving that the radiometric phenomenon is caused by the interaction between the heated side of the vane and the gas. The kinetic theory explanation given by Reynolds is in fact a free molecule approximation of the radiometric effect: the molecules colliding with the hot side leave with an increased velocity relative to those colliding with the cold side. This leads to a larger momentum change on the hot side, and results in the motion of the vanes with the hot side trailing.

The situation is, however, different in transitional or near-continuum flow. The molecules with higher velocities leave the hot side of the vane and collide with incoming molecules. These collisions cut the surface flux more efficiently than those reflected on the cold surface [8]. Essentially, this means that these effects compensate each other, and pressures in the center of the vane are equal. This theory was first proposed by Reynolds [8]. At about the same time, Maxwell [9] also showed that an unbalanced force exists near the edge of the heated side of the vane, where the heat flow in the gas is nonuniform. Almost 50 years later, Einstein presented a simple theory [10] that related the force on the vanes to their perimeter. This edge dependence of the vane force has found partial confirmation in experimental work [11], where the force was found to depend on perimeter, although not to the extent Einstein has predicted. Since about that time, the edge theory has become widely accepted.

The inversely proportional dependence of the radiometric force of a vane placed in a temperature gradient, derived in [10], is similar to the high-pressure part of the general dependence proposed by Brüche and Littwin [12] that combines both high and low-pressure regimes as

$$F = \frac{1}{(a/p) + (p/b)}. \tag{1}$$

This expression reflects the fact that the radiometric force has a maximum at some pressure that depends on gas and geometric properties, quantitatively shown as early as 1919

[13]. At low pressures, a free-molecular area force is the dominant one, with the force increasing with pressure. At high pressures, the collisional edge force becomes dominant, and the force decreases as pressure increases.

The phenomenon that drives Crookes' radiometer has been summarized by Draper [14] who in effect described our present understanding of it. A temperature gradient exists on the surface if tangential stresses are to arise. These stresses are the result of thermal transpiration, with the gas moving over the surface from the cold to the hot side. Following this explanation [14], the principal force that contributes to the rotation of the vanes in the pressure regime where the radiometer is most effective, is the force created near the edges (a zone with the dimensions of a mean-free path λ, according to [10]). Among the studies that appeared during the second half of the last century, research papers on the subject [15,16] need to be mentioned, whereas most other publications consisted of historic analyzes and overviews.

Interest in radiometric phenomena started to grow rapidly in the last decade, primarily because the radiometric phenomena were found to be useful in a number of different micro- and large-scale devices. One of the most important of these is atomic force microscopy (AFM), a research field that, although invented back in 1986 [17], has been brought to the forefront of the modern nanotechnologies in the last several years (see, for example, [18–20]). The temperature of an AFM cantilever can increase due to resistive heating under piezoelectric excitation or due to heating by a laser that senses the cantilever displacement. For low-pressure AFM, the radiometric force (or, as it is often referred to in AFM literature, Knudsen force) is generated by thermally induced rarefied gas flow. This radiometric force can also affect AFM measurements of heated samples. On the other hand, the occurrence of radiometric force in heated AFM cantilevers can provide thermal actuation for mass detection, thermogravimetry, heat-flow measurements, and thermal processing through local heating on submicron scale [21].

The radiometric force in application to modern microactuators has been studied in [22], where the direct simulation Monte Carlo (DSMC) method [23] was used to model forces on vanes mounted on an armature. This method, along with experimental measurements, has been employed in [24] to study a concept of an optomicroengine that uses radiometric forces. Subsequently, Passian with co-workers have examined radiometric phenomena both experimentally and analytically (see, for example, [25,26]), mostly with application to microcantilevers. The use of radiometric forces as an approach to study gas-surface translational energy accommodation has been suggested by Passian *et al.* in [27]. A new concept of a high-altitude aircraft supported by microwave energy that uses radiometric effects has also been put forward in [28].

The above referenced modern studies of radiometric phenomena have been supported by modern measurement technologies that allow higher accuracy and by state-of-the-art numerical methods that rely heavily on parallel computing. These two factors, along with the revived interest in the application of radiometric phenomena, have prompted the authors to revisit the contribution of the "collisionless" (area) versus the "collisional" (edge) forces to the total radiometric force.

The main objective of this work is to examine experimentally radiometric forces created by rarefied gas flows on heated plates of different shapes, and to analyze numerically the change in the total force as a function of gas pressure. While experimental measurement of the radiometric force has benefits of correctly accounting for different factors, such as gas-surface accommodation, internal structure of molecules, and complex three-dimensional geometries, numerical modeling provides detailed information of gas flow properties.

Three radiometer vane geometries were used in the experiments, and each consisted of a Teflon insulator placed between two aluminum plates. A resistive heater was located between one of the plates and the Teflon insulator, and the temperature of the hot side of the device was maintained by varying the power input to the heater. Each of the plates and insulator are 0.32 cm thick, and when assembled yield a device thickness of 0.95 cm. The first device was a circle 11.1 cm in diameter, the second device was a rectangle with the same area and dimensions of 7.62×12.7 cm^2, and the third was a smaller circular vane with a diameter of 8.6 cm with an area and perimeter smaller than both of the previous devices.

Each of these devices was individually mounted on a modified nano-Newton thrust stand (nNTS) [29] located inside of a 3.0 m diameter vacuum chamber. Here, the mounting was accomplished with a much smaller attachment than in previous work [30], where a small threaded rod of dimension 0.22×4 cm^2 was used. When calibrated using a set of electrostatic combs [31], the nNTS provides very accurate and repeatable data with typical force resolution of approximately 0.1 μN and statistical scatter around 1%.

Experimental data were obtained for each device by evacuating the chamber to a base pressure below 10^{-3} Pa. A constant voltage was applied to the resistive heater, which was affixed by a pressure sensitive adhesive and only slightly smaller in diameter than the vane itself. This resulted in the main radiometer surfaces reaching temperatures of approximately 419 K (hot) and 394 K (cold), although these values varied somewhat for the different devices tested. A finite element thermal model was used to confirm that the high conductivity of the aluminum surfaces and the large size of the heating element led to a variation in temperature over the surface of each plate of ≤ 0.1 K. Actual temperature measurements were taken continually very near the edges of both the hot and cold sides as force measurements were being made for each pressure tested. As small variations (≤ 0.5 K) between the hot and cold plates occurred due to varying background pressures, results presented are normalized by the temperature difference between the hot and the cold plates (ΔT) at the time each force measurement was made. Verification of this normalization method has been conducted for temperature differences varying from 4 to 30 K, and an exceptional linearity of the radiometric force with ΔT was observed. Note that this result indirectly verifies the measurements of [32] for a microcantilever. The background pressure inside the chamber was varied from 0.1 to 1.2 Pa, where both the upper and lower bounds were limited by the pumping capacity of the facility used. Argon was utilized as the test gas.

The use of a kinetic approach is necessary to model radiometric flows, as it would allow one to properly account for rarefaction effects, such as thermal stresses in the gas and thermal slip on the surface [33]. At present, the DSMC method is the most powerful and widely used kinetic approach to the solution of the Boltzmann equation, the main equation for dilute gases. The DSMC method is a statistical, particle-based approach, which fundamental principle is the splitting of continuous motion and collisions of molecules at a time step Δt into two sequential stages: free-molecular transfer and collision relaxation. This approach however suffers from high computational cost compared to the conventional computational fluid dynamics (CFD) methods for solving continuum flow problems. The computational cost of DSMC is especially significant for low speed flows, where it is impacted by flow dimensionality, long time to reach steady state, low signal-to-noise ratio, multiple physical scales usually involved, and other factors.

There is a number of alternative DSMC-based approaches proposed to deal with the problem of low signal-to-noise ratio that allow significant reduction in macroparameter sampling time compared to the standard DSMC method (see, for example, [34,35]). Although all these techniques do allow significant reduction in the steady-state time averaging cost, they do not deal with the reduction in computational cost associated with the long time to reach steady state, which is often the main issue for modeling low speed flows. A plausible numerical alternative for such flows is a deterministic solution of a simplified form of the Boltzmann equation known as a kinetic model equations. In these equations, the complex collision integral of the Boltzmann equation is replaced by a simplified model that provides an approximation of the collisional relaxation of the velocity distribution function. Bhatnagar-Gross-Krook (BGK) [36] and ellipsoidal statistical (ES) [37] kinetic models use a nonlinear relaxation term instead of the full Boltzmann collision integral, and possess the same collision invariants as the Boltzmann equation. Both BGK and ES models satisfy the Boltzmann's H theorem expressing the increase in entropy of the gas under consideration. Kinetic models should also reproduce the gas transport coefficients—viscosity, thermal conductivity, and species diffusivity—resulting from the Boltzmann equation. The primary advantage of this numerical alternative is its high computational efficiency.

In this work, the numerical solutions were obtained with two kinetic approaches, the DSMC method using the SMILE computational tool [38], and a finite difference solution of the ES-BGK kinetic equation. The two-dimensional (2D) flow over a 0.95×3.81 cm^2 rectangular plate placed in the center of a 0.45×45 cm^2 chamber was modeled in 2D. The DSMC computations typically used about 250 000 cells, 2×10^6 molecules, and ran about 2×10^6 time steps to achieve acceptable statistical accuracy. The variable hard sphere (VHS) model of molecular interaction was used with parameters listed in [23]. Three-blocks nonuniform rectangular grid was used in the solution of the ES-BGK equation with the total of 13 359 spatial nodes. The Gauss-Hermite quadrature of order 16 and three-eighths rule were used for discretization of velocity magnitude and angle, respectively. The VHS model viscosity-temperature dependence was used.

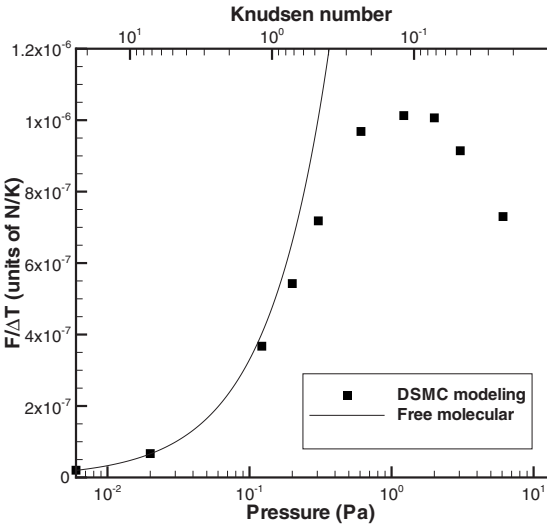

FIG. 1. Computed force on small rectangular plate in argon.

Both approaches were using fully diffuse model for gas-surface interaction.

Note that the linear size of the chamber in the computations was almost an order of magnitude smaller than in the experiments. Even for the small chamber, a single DSMC run took days on a parallel computer, and modeling a full experimental setup would be impractical from the computational standpoint. Although using a smaller chamber and, in the absence of known accommodation laws, assuming a fully diffuse reflection of molecules on the surface, prevents direct comparisons with the data, it does allow for a qualitative analysis of the flow and force behavior. Also, although the DSMC method is applicable to the entire range of flow regimes from free molecule to continuum, computations at high pressures (Knudsen numbers on the order of 0.01 and below) are extremely computationally expensive, and were not conducted in this work. The high-pressure flows are challenging to compute with the model kinetic equations as well, as the time to reach steady state drastically increases, therefore limiting the application of the present single-processor ES-BGK code.

The total radiometric force on the smaller rectangular plate in argon, computed with DSMC for a range of gas pressures, is presented in Fig. 1. The results clearly follow the behavior described by Eq. (1), where the computed data peaks at a pressure of approximately 1 Pa, which corresponds to a Knudsen number around 0.1 based on the plate length. For lower pressures, the numerical results are compared to the analytic free-molecular expression [39].The results agree very well for Knudsen numbers of about 10 and higher, but start to deviate at lower Kn. At lower Knudsen numbers, molecular collisions start to increase the energies of incident molecules, therefore degrading the radiometric force. As the Knudsen number decreases, thermal transpiration effects start to appear, driving gas from colder walls to the hotter ones. Although in a simple scenario of a cold-to-hot motion the thermal transpiration should increase the force, the actual flow is much more complex, as colder chamber wall may also play a role (see, for example, [40]). Note that the above comparisons have been conducted for

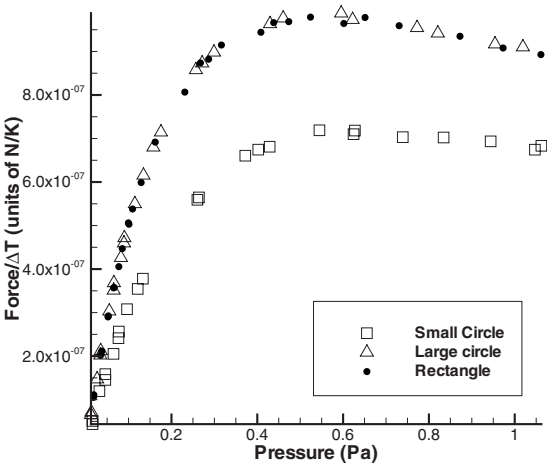

FIG. 2. Measured force on three different plates in argon.

the other gases (helium and nitrogen) and similar patterns were observed.

The results of the experimental study of different radiometer shapes are summarized in Fig. 2. The experimental error based on standard deviation ranges from a few percent at the lowest pressures to less than 1% through most of the curve. However, due to the normalization by experimental temperature measurements and the small uncertainty of the calibration method, the total absolute experimental uncertainty is ~4%. Day-to-day variation in multiple data sets has been observed to be ~1%. The results show that the forces on the rectangular and large circular plate are very close, while that on the lower circular plate is systematically lower.

To provide more quantitative analysis of the data, the results are also shown as ratios in Fig. 3 (polynomial approximations of experimental points were used to provide values at fixed pressures). It is clearly seen that in the low-pressure region the force is proportional to the plate area. This is decidedly consistent with predictions made by free-molecular theory. As the flow transitions from the collisionless regime, the picture becomes distinctly more complex. While it is readily observed that the plates with larger area produce more force at their respective peaks, the force-area

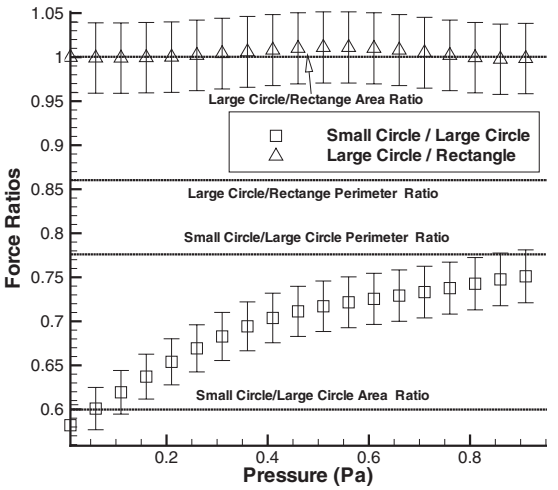

FIG. 3. Comparison of force ratios for two geometry pairs.

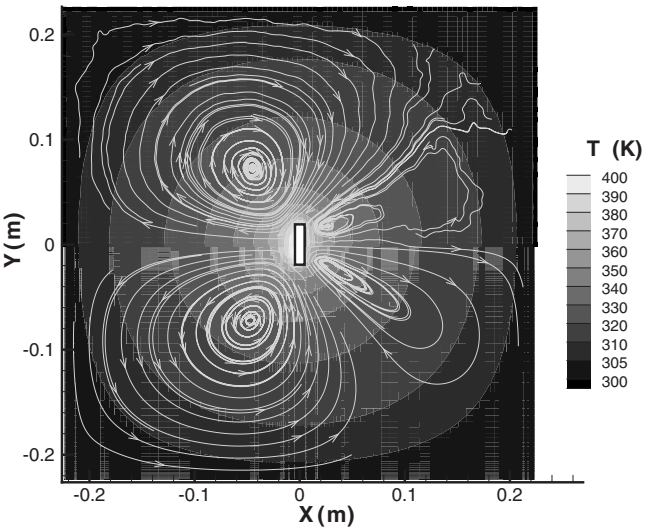

FIG. 4. DSMC (top) and ES-BGK (bottom) streamlines and temperature field in helium.

ratio does not hold. When comparing the peaks of the large and small circular plates, it is found that small plate creates 72% of the force of the larger one. Interestingly, this is between the area ratio (60%) and the perimeter ratio (77%). Though it is tempting to presume that the perimeter force was beginning to dominate, it is not obvious that this is the case. The uncertainty stems from comparison of the larger vane data, where the force produced by the circle is decidedly similar to that of the large rectangle. It seems quite contradictory to accepted theory that a device with 14% less perimeter would create a nearly identical force without an equivalent increase in heated surface. This unexpected result may be explained by more efficient pressure redistribution in front of the circular plate due to vortices, where the vortex structure and pressure distribution are discussed below.

The vortex structure computed with DSMC (top) and ES-BGK (bottom) for helium at 2 Pa is illustrated in Fig. 4. Although qualitatively similar results were observed for argon, helium results are shown here since the vortices are noticeably more pronounced for the lighter gas. Two large counterpropagating vortices are formed in front of the hot wall, and two small vortices are created near the cold surface. The vortex structure qualitatively agrees with that of [24], but is generally more complex than that described by Kennard [41]. It appears to be driven by the thermal transpiration caused by the temperature differences on the plate edges and the chamber walls. The maximum flow velocity is about 5 m/s in front of the hot wall and 1.5 m/s for the cold wall. Let us remind that these numbers are obtained for a two-dimensional flow. The DSMC computations conducted for the corresponding axially symmetric flow show qualitatively similar pattern, but indicate that the maximum flow velocity in front of the hot and cold wall is about 7 and 3 m/s, respectively. Since higher vortex velocity generally results in larger pressures in front of the plate, this may in part explain small difference between the circular and rectangular plates observed in the experiments. The temperature field, also given in Fig. 4, shows that near the chamber walls the gas temperature is several degrees higher than the wall tem-

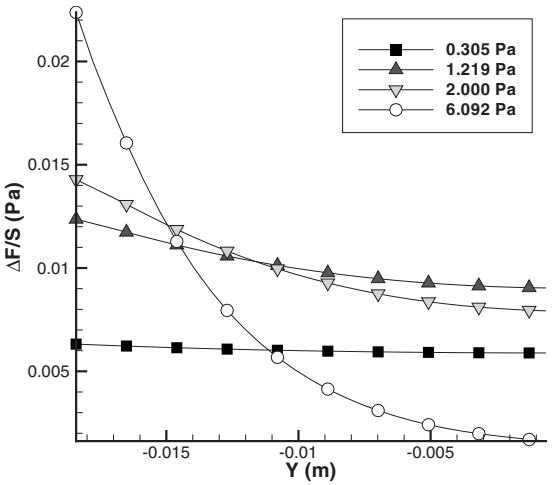

FIG. 5. Computed pressure difference along the plate.

perature of 300 K. This nonequilibrium between the gas and the chamber wall indicates that the chamber size impacts the flow around the plate.

To further explore the dependence of the radiometric force on area and perimeter, pressure distributions on the plate surface have been calculated using the two kinetic approaches. The difference between pressure on the hot side and pressure on the cold side obtained through the solution of the ES-BGK equation is presented in Fig. 5 for argon gas. Only a half of the plate is shown due to the symmetry of the flow, and $Y=0$ corresponds to the center of the plate. The presented pressure difference essentially determines the magnitude of the radiometric force. Note that the DSMC results are close to ES-BGK, although they have noticeable statistical scatter and are not shown here. For the lowest pressure of 0.305 Pa, the pressure difference, as well as individual distributions over the cold and hot surfaces, is nearly flat. This indicates that free-molecular effects dominate at this pressure, even though based on the Knudsen number ($\mathrm{Kn}\approx 0.5$) the system is far from free molecular. As pressure increases, pressure difference near the edges becomes larger than at the center, thus showing that the "collisional" thermal transpiration forces become noticeable. It is important that (i) the pressure difference is still relatively flat near 1.2 Pa where the force is maximum, and (ii) the impact of the edges propagates much further than a single mean-free path, essentially increasing the importance of the vane area. These statements hold for all gases under consideration.

In conclusion, the experimental and computational study has shown that although the influence of the edge effects increases with pressure, the radiometric force is mostly governed by area and not edge effects for pressures where this force is maximum. Although geometric and temperature parameters considered here are somewhat different from those in a typical Crookes radiometer, the authors believe that this conclusion holds for it as well. A number of other important effects, not addressed in this paper, such as the shear force of the side walls of the vane, the effect of the chamber walls, and the influence of surface roughness and vane perforation, will be a topic of future research.

[1] A. E. Woodruff, Isis **57**, 188 (1966).
[2] A. Bennet, Philos. Trans. R. Soc. London **82**, 81 (1792).
[3] A. Fresnel, Ann. Chim. Phys. **29**, 57 (1825).
[4] W. Crookes, Philos. Trans. R. Soc. London **163**, 277 (1873).
[5] W. Crookes, Philos. Trans. R. Soc. London **165**, 519 (1875).
[6] O. Reynolds, Philos. Trans. R. Soc. London **166**, 725 (1876).
[7] A. Schuster, Philos. Trans. R. Soc. London **166**, 715 (1876).
[8] O. Reynolds, Philos. Trans. R. Soc. London **170**, 727 (1879).
[9] J. C. Maxwell, Philos. Trans. R. Soc. London **170**, 231 (1879).
[10] A. Einstein, Z. Phys. **27**, 1 (1924).
[11] H. E. Marsh, J. Opt. Soc. Am. **12**, 135 (1926).
[12] E. Brüche and W. Littwin, Z. Phys. **52**, 318 (1928).
[13] W. H. Westphal, Z. Phys. **1**, 92 (1920).
[14] C. W. Draper, J. Chem. Educ. **53**, 357 (1976).
[15] E. A. Mason and B. Block, Ann. Phys. **37**(1), 7 (1966).
[16] F. S. Crawford, Am. J. Phys. **53**, 1105 (1985).
[17] G. Binnig, C. F. Quate, and C. Gerber, Phys. Rev. Lett. **56**, 930 (1986).
[18] F. Giessibl, Rev. Mod. Phys. **75**, 949 (2003).
[19] P. Hinterdorfer and Y. F. Dufrêne, Nat. Methods **3**, 347 (2006).
[20] B. Gotsmann and U. Durig, Appl. Phys. Lett. **87**, 194102 (2005).
[21] B. A. Nelson and W. P. King, *Applied Scanning Probe Methods IV* (Springer, Berlin, 2006), pp. 251–275.
[22] D. C. Wadsworth and E. P. Muntz, J. Microelectromech. Syst. **5**, 59 (1996).
[23] G. A. Bird, *Molecular Gas Dynamics and the Direct Simulation of Gas Flows* (Clarendon Press, Oxford, 1994).
[24] M. Ota, T. Nakao, and M. Sakamoto, Math. Comput. Simul. **55**, 223 (2001).
[25] A. Passian, A. Wig, F. Meriaudeau, T. L. Ferrell, and T. Thundat, J. Appl. Phys. **92**, 6326 (2002).
[26] A. Passian *et al.*, Ultramicroscopy **97**, 401 (2003).
[27] A. Passian, R. J. Warmack, T. L. Ferrell, and T. Thundat, Phys. Rev. Lett. **90**, 124503 (2003).
[28] G. Benford and J. Benford, Acta Astronaut. **56**, 529 (2005).
[29] A. J. Jamison, A. D. Ketsdever, and E. P. Muntz, Rev. Sci. Instrum. **73**, 3629 (2002).
[30] N. Selden, C. Ngalande, S. Gimelshein, and A. Ketsdever, AIAA Pap., 4403 (2007).
[31] N. P. Selden and A. D. Ketsdever, Rev. Sci. Instrum. **74**, 5249 (2003).
[32] A. L. Lereu, A. Passian, T. L. Ferrell, and T. Thundat, Appl. Phys. Lett. **84**, 1013 (2004).
[33] A. A. Alexeenko, S. F. Gimelshein, E. P. Muntz, and A. D. Ketsdever, Int. J. Therm. Sci. **45**, 1045 (2006).
[34] J. Fan and C. Shen, J. Computat. Phys. **167**, 393 (2001).
[35] C. R. Kaplan and E. S. Oran, AIAA J. **40**, 82 (2002).
[36] P. L. Bhatnagar, E. P. Gross, and M. A. Krook, Phys. Rev. **94**, 511 (1954).

[37] L. H. Holway, Rarefied Gas Dyn. **1**, 193 (1966).
[38] M. S. Ivanov, S. F. Gimelshein, and G. N. Markelov, Comput. Math. Appl. **35**, 113 (1998).
[39] S. Dushman, *Scientific Foundations of Vacuum Technique* (Wiley, New York, 1949).
[40] K. Aoki, Y. Sone, and Y. Waniguchi, Comput. Math. Appl. **35**, 15 (1998).
[41] E. H. Kennard, *Kinetic Theory of Gases* (McGraw-Hill, New York, 1938).